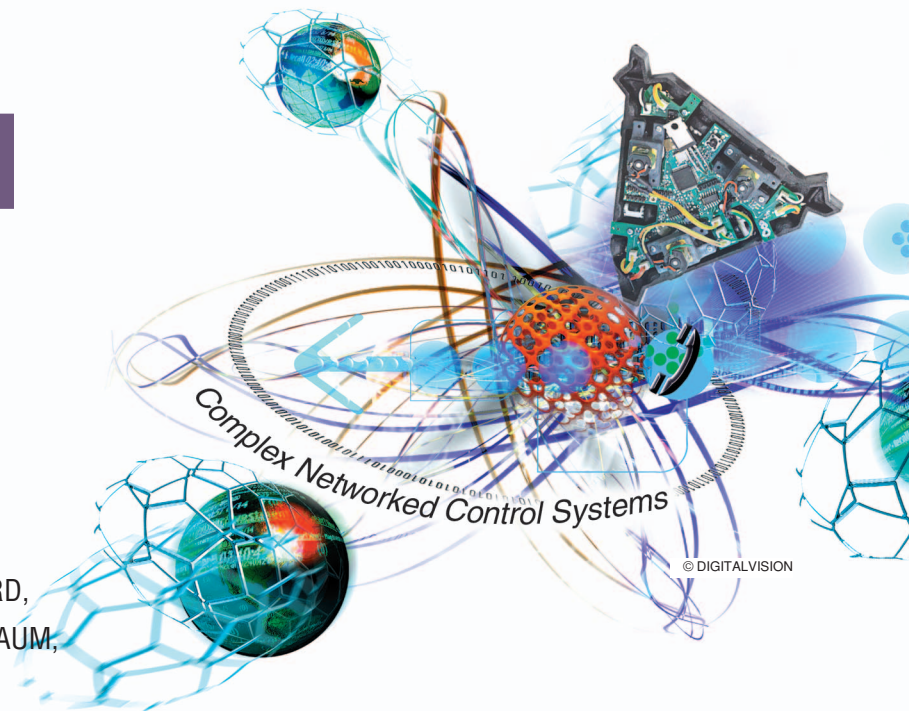


# Oscillator Models and Collective Motion

DEREK A. PALEY, NAOMI EHRICH LEONARD,  
RODOLPHE SEPULCHRE, DANIEL GRÜNBAUM,  
and JULIA K. PARRISH



## SPATIAL PATTERNS IN THE DYNAMICS OF ENGINEERED AND BIOLOGICAL NETWORKS

**C**oupled-phase oscillator models are used to study the behavior of many natural and engineered systems that represent aggregations of individuals. Examples include the heart's pacemaker cells [1, pp. 268–278], neurons in the brain, a group of fireflies, the central nervous system in a lamprey eel [2], and an array of superconducting Josephson junctions [3]. In all of these cases, the activity of each individual is periodic; for example, each individual firefly, neuron, or pacemaker cell flashes or fires at regular intervals. To investigate how the dynamics of interacting individuals can converge to a synchronized collective state, that is, flashing or firing in unison, each individual is modeled as an oscillator, while the collective is modeled as a network of coupled oscillators [4], [5]. The network model relies on interaction among the individuals; if individual A is coupled to individual B, then individual A adjusts its oscillation in response to what individual B is doing. For example, a firefly modifies the frequency of its flashing in response to the flashing activity of its neighbors. With the right kind of interaction, the model reveals how the whole firefly group can converge to synchronous flashing.

Synchronization refers to the situation in which all of the oscillators have the same phase. However, coupled oscillators often exhibit a different and interesting family of equilibria called *incoherent states* [6]. In some incoherent states, the oscillator phases are distributed around the unit circle such that their centroid is at the origin. Since the phases balance themselves around the unit circle, we refer to these states as *balanced states*. In biological systems such as fish schools, synchronization and balancing have different implications not only for group characteristics such as movement, but also for the capacity of groups to fulfill biological roles such as predator avoidance, social foraging, and mate selection.

For modeling, analysis, and synthesis of collective motion, we describe a framework called particles with coupled oscillator dynamics (PCOD), which extends coupled oscillator dynamics to include spatial dynamics. The phase of each oscillator defines the direction of a particle moving in the plane at constant speed. Note that, for circular motion at a constant speed, the motion of each particle can be identified with its direction of travel since at regular intervals the particle is instantaneously heading north. Synchronization in a spatial framework implies that, at all

**The synthesis problem is to design a steering control for each particle  
so that desired collective spatial patterns emerge.**

times, all of the particles have the same direction of motion. On the other hand, collective motion with balanced phases has a fixed center of mass. For example, when two particles head in opposite directions, their phases are balanced and their center of mass is at rest. PCOD allows for limited inter-particle interaction, which is fixed and undirected. In [7], we describe extensions to PCOD that allow for time-varying, directed interactions, which arise, for example, when individuals communicate only with spatial neighbors.

The synthesis problem is to design a steering control for each particle so that desired collective spatial patterns emerge. Examples of such steering controls include control laws that can stabilize parallel motion as well as control laws that stabilize the circular motion of all particles in a symmetric pattern. For a class of spatial patterns, we address the inverse problem, that is, given a spatial pattern, we specify fixed interaction that produces the desired pattern. Likewise, we analyze spatial pattern bifurcations, which are changes in group motion that occur as a result of changing system and control parameters.

These ideas are applicable to engineered mobile sensor networks and to the study of animal aggregations. For the former, the inverse problem results make it possible to systematically design control laws that yield sensor network patterns that optimize information content in the sampled data [8]. For animal aggregations, the inverse problem results and bifurcation analyses make it possible to develop and study simple models of interaction rules that yield group behavior resembling field observations.

One application to engineered mobile agent collectives is the problem of mobile sensor network design for search, mapping, or environmental monitoring. At-sea demonstrations of coordinated control strategies for formations of underwater mobile sensors are described in [9] and [10]. Likewise, many open questions exist in the study of emergent behavior in biological collectives, in part because of variation across species [11]–[14]. Related work on collective motion from the engineering and physics literature includes [15]–[18].

In the next section, we first present the oscillator model with spatial dynamics. We make the connection between phase synchronization and linear momentum of the group and describe how to design stabilizing steering control laws by taking the gradient of a phase potential. These concepts are generalized to the case of fixed, limited communication by means of interaction networks and the quadratic form induced by the Laplacian matrix. Sta-

bilization results are summarized, and application to design of patterns for sensor coverage by mobile sensor networks is discussed.

In the second half of this article, we use the coupled oscillator model with spatial dynamics to study biological collectives. We show how the particle model resembles a model used to study animal aggregations [19], [20]. We use this analogy to examine collective motion of the particle model and show how parameters can be varied to produce a rich set of complex behaviors. We then use the phase potential defined by the model to analyze fish-population data (see “Analysis of Fish Data”), specifically, giant danios moving about in a 1 m<sup>3</sup> tank [20]–[22]. As a preliminary step, we present two-dimensional analyses of processes that are typically three-dimensional (3D) in nature. We conclude with a brief prospectus on the joint pursuits of engineering analysis by biologists and biological analysis by engineers (see “Collaborative Engineering and Biological Analysis”).

## OSCILLATOR MODEL AND COLLECTIVE MOTION

PCOD provides a common mathematical framework for describing collectives of autonomous robots and biological organisms. In PCOD, the collective dynamics are defined by a particle model in which each individual is represented by a particle (point mass). The particle model describes the motion of  $N$  identical individuals defined by their positions and directions of motion. We assume that the particles have unit mass, travel at unit speed, and can maneuver by steering but not by speeding up or slowing down.

To illustrate the connection to coupled oscillator dynamics, we identify the complex plane  $\mathbb{C}$  with  $\mathbb{R}^2$  and use complex notation to describe each particle’s position and velocity. For  $k = 1, \dots, N$ , the position of the  $k$ th particle is  $r_k = x_k + iy_k \in \mathbb{C}$ , while the velocity of the  $k$ th particle is  $e^{i\theta_k} = \cos \theta_k + i \sin \theta_k$ , where  $\theta_k$  is the phase of the  $k$ th particle. Each phase  $\theta_k$  represents a point on the unit circle  $S^1$ , which is the space of angles. The collection of all of the phases evolves on the  $N$ -torus  $\mathbb{T}^N$ , which is equal to  $S^1 \times \dots \times S^1$  ( $N$  times). Let  $\mathbf{r} \triangleq (r_1, \dots, r_N)^T \in \mathbb{C}^N$  and  $\boldsymbol{\theta} \triangleq (\theta_1, \dots, \theta_N)^T \in \mathbb{T}^N$ . The steering control  $u_k$ , which is a feedback control law, is a function of  $\mathbf{r}$  and  $\boldsymbol{\theta}$ . With this notation, the particle model is [15]

$$\dot{r}_k = e^{i\theta_k}, \quad (1)$$

$$\dot{\theta}_k = u_k(\mathbf{r}, \boldsymbol{\theta}), \quad k = 1, \dots, N. \quad (2)$$

## Investigation of collective motion represents an overlap of interests between engineers and biologists who are motivated by different scientific questions.

The fact that the phase  $\theta_k$  of particle  $k$  represents a point on  $S^1$  distinguishes the model (1), (2) from the particle model used in [16], which describes the orientation of particle velocity by a real number in the interval  $[0, 2\pi)$ . Note that in (2),  $\theta_k$  is not confined to a bounded interval;  $\theta_k$  can be seen to evolve in  $S^1$  by identifying  $\theta_k$  with  $\theta_k + 2\pi$ . On  $\mathbb{T}^N$ , the control  $u_k$  is a  $2\pi$ -periodic vector field, that is, for all  $\mathbf{r}, \boldsymbol{\theta}$ ,  $u_k(\mathbf{r}, \boldsymbol{\theta} + 2\pi\mathbf{1}) = u_k(\mathbf{r}, \boldsymbol{\theta})$ , where  $\mathbf{1} \triangleq (1, \dots, 1)^T \in \mathbb{R}^N$ . Modeling on the torus leads to global results such as Theorem 1 below, while modeling on the real line can provide only local results since the configuration space is not Euclidean.

If, for all  $k = 1, \dots, N$ , the control  $u_k$  is identically zero, then each particle travels in a straight line in its initial direction  $\theta_k(0)$ . If, on the other hand, for all  $k = 1, \dots, N$ ,  $u_k \triangleq \omega_0$  is constant but not zero, then each particle travels around a circle with radius  $|\omega_0|^{-1}$ . The direction of rotation around the circle is determined by the sign of  $\omega_0$ . In particular, if  $\omega_0 > 0$ , then all particles rotate counterclockwise, whereas, if  $\omega_0 < 0$ , then all particles rotate clockwise. The center of the  $k$ th circle is

$$c_k \triangleq r_k + \omega_0^{-1} i e^{i\theta_k}, \quad (3)$$

while the center of mass of the particle group is

$$R \triangleq \frac{1}{N} \sum_{j=1}^N r_j. \quad (4)$$

The particle model (1), (2) describes a second-order Newtonian model of  $N$  point masses, each of which is subject to a force orthogonal to its velocity. Note that, for all  $k = 1, \dots, N$ ,  $\ddot{r}_k = u_k i \dot{r}_k$ , which implies that the total kinetic energy is conserved, since  $(d/dt)(1/2)|\dot{r}_k|^2 = \langle \dot{r}_k, \ddot{r}_k \rangle = 0$ , where  $\langle x, y \rangle \triangleq \text{Re}\{x^* y\}$  and  $*$  denotes the conjugate transpose. Total linear momentum, which is proportional to the velocity  $\dot{R}$  of the center of mass, is not conserved. In fact, control of total linear momentum plays a role in the design methodology described below.

Let  $r_{kj} \triangleq r_k - r_j$  and  $\theta_{kj} \triangleq \theta_k - \theta_j$  denote, respectively, the position and phase of particle  $k$  relative to particle  $j$ . A shape control for particle  $k$  depends only on the shape variables  $\theta_{kj}$  and  $r_{kj} e^{-i\theta_k}$  for all  $j = 1, \dots, N$ . The closed-loop particle model with shape control is invariant to rigid rotation and translation of the collective [15]. Since rigid translation of the collective exercises two degrees of freedom while rigid rotation of the collective exercises one degree of freedom, the closed-loop dynamics evolve on shape space,

which is a reduced configuration space that has three fewer dimensions than the full configuration space.

Equilibria of the dynamics in shape space are called *relative equilibria* of the full space. Two types of relative equilibria of the particle model are parallel formations and circular formations. Particles in a parallel formation travel in a constant, identical direction, which means  $\dot{\theta}_k = 0$  and  $\theta_k = \theta_j$  for all pairs  $j$  and  $k$ . Particles in a circular formation travel around the same circle in the same direction, which means  $\dot{\theta}_{kj} = 0$  and  $c_k = c_j$  for all pairs  $j$  and  $k$ . One of our goals is to derive shape controls that provably stabilize these formations for  $N \geq 2$ .

### Phase Model

As a first step in designing steering controls for the particle model, we independently consider the subsystem of phases. To do this, we split the control  $u_k$  into three terms, specifically,

$$u_k = \omega_0 + u_k^{\text{spac}}(\mathbf{r}, \boldsymbol{\theta}) + u_k^{\text{ori}}(\boldsymbol{\theta}), \quad k = 1, \dots, N, \quad (5)$$

where  $\omega_0 \in \mathbb{R}$  is a constant,  $u_k^{\text{spac}}(\mathbf{r}, \boldsymbol{\theta})$  is the spacing control, and  $u_k^{\text{ori}}(\boldsymbol{\theta})$  is the orientation control. By ignoring the particle positions and setting  $u_k^{\text{spac}} = 0$ , we obtain the phase model

$$\dot{\theta}_k = \omega_0 + u_k^{\text{ori}}(\boldsymbol{\theta}), \quad k = 1, \dots, N, \quad (6)$$

which is a system of coupled-phase oscillators with identical natural frequency  $\omega_0$ . In general, the orientation control  $u_k^{\text{ori}}$  depends on the phases  $\theta_1, \dots, \theta_N$ . If  $u_k^{\text{ori}}$  is a shape control, then  $u_k^{\text{ori}}$  depends only on the relative phases  $\theta_{kj}$ , and the phase model is invariant to rigid rotation of all of the phases.

The phases  $\theta_j$  and  $\theta_k$  are phase locked if  $\dot{\theta}_{kj} = 0$ . A synchronized phase arrangement  $\boldsymbol{\theta}$  is a phase-locked arrangement for which  $\theta_k = \theta_j$  for all pairs  $j$  and  $k$ , which implies that the particles are in a parallel formation. The phase order parameter  $p_\theta$ , which is a measure of synchrony of coupled-phase oscillators, is defined by [5]

$$p_\theta \triangleq \frac{1}{N} \sum_{j=1}^N e^{i\theta_j}. \quad (7)$$

The magnitude  $|p_\theta|$ , which satisfies  $0 \leq |p_\theta| \leq 1$ , is proportional to the level of synchrony of the phases; in particular,  $|p_\theta| = 1$  for synchronized phases. A balanced phase

## Analysis of Fish Data

Evidence of phase synchronization has been found in actual fish schooling data by computing the value of the Laplacian phase potential  $W_1(\theta)$ . Phase synchronization is characterized by small values of  $W_1(\theta)$  given by (12) with  $L = L^{\text{ori}}$ . Recall that  $W_1(\theta)$  is nonnegative for directed or undirected graphs and zero if  $\theta$  is synchronized. Even if the interaction network is not connected,  $W_1(\theta) = 0$  only if the phases within each connected subgraph are synchronized.

We examine trajectories of individual fish within four-fish and eight-fish populations of giant danios (*danio aequipinnatus*). The trajectories are recorded using stereo videography and a computerized tracking algorithm; see [20] for details on the data collection. Each experiment contains ten minutes of data collected in a 1-m<sup>3</sup> tank, shown in Figure S1. Continuous fish trajectories are generated from the raw data using smoothing splines to remove frame-rate noise. We calculate smoothed unit-velocity estimates by averaging over a five-second moving window. We use only the horizontal components of position and velocity, which is appropriate for an initial analysis because many of the spatial patterns evident in these data are primarily two dimensional [21].

As a first step, we calculate  $W_1(\theta)$  using the switching interaction network generated from the realistic orientation zones defined in [20]. A typical body length for a giant danio is 5.3 cm, which we denote by  $b$ . The orientation zone of the  $k$ th fish is contained in the annulus defined by  $\{r \mid 1.4b \leq |r - r_k| \leq 2.4b\}$  and with the trailing blind spot  $\alpha_k = 60^\circ$ . A snapshot of each data set is shown in Figure S2 with orientation zones shown in gray. The four-fish data set exhibits periods of highly synchronized collective motion. The two eight-fish data sets, panels (b) and (c) in Figure S2, exhibit markedly different schooling behavior that we refer to as *tight-milling* and *diffuse-milling*, respectively. For this type of interaction network,

low values of the phase potential are generated if the orientation zones are mostly empty, as in the case of diffuse-milling.

To overcome this limitation, we recalculate the Laplacian phase potential using an interaction network generated by the nearest  $n$  neighbors of each fish. In the left column of Figure S3, we plot the potential  $W_1(\theta)$  scaled by  $(2/n + 1)$  so that the resulting magnitude is in the interval  $[0, 1]$  for all  $n$ . In each panel, we plot the results for  $n = 1$  and  $n = N - 1$  for a representative 30 s period starting from  $t = 30$  s. In the right column of Figure S3, we plot the histograms of the scaled potentials for all 10 min of each



**FIGURE S1** Tight-milling eight-fish experiment. (a) 1-m<sup>3</sup> tank experimental enclosure with eight giant danios; note the solitary fish near the top of the tank. (b) Close-up view of seven of the eight fish swimming in a highly polarized school.

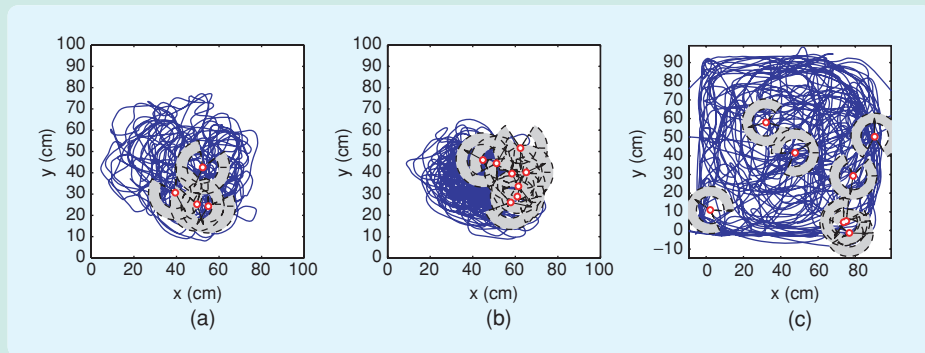


**FIGURE S2** Actual fish school trajectories and estimated perceptual zones. The position (red circle), direction of motion (black arrow), trajectory (blue line), and orientation zone (gray patch) are plotted for each fish. (a) The four-fish experiment is characterized by polarized motion; (b) the tight-milling eight-fish experiment is characterized by small inter-fish spacing; (c) the diffuse-milling eight-fish experiment is characterized by large inter-fish spacing, which leads to predominantly empty neighbor sets in the orientation directed graph.

data set for  $n = 1$  and  $n = N - 1$  as well as the histogram of the difference between the two values of the phase potential. For  $n = 1$ , if the nearest neighbor is in the zone of repulsion  $\{r \mid |r - r_k| \leq 1.4b\}$ , we use the second nearest neighbor. Note that  $n = N - 1$  corresponds to the complete graph, in which case  $(2/n + 1)W_1(\theta) = 1 - |\rho_\theta|^2$  by (13) and (8). This metric is inversely related to the mobility of the center of mass of the group, which may be constrained by the size of the tank.

Using the histograms in Figure S3, we make the following observations. The four-fish data possess a bimodal distribution of the scaled phase potential histogram for  $n = N - 1$ . The peak near zero corresponds to synchronized collective motion. The peak at 0.75 corresponds to several nearly synchronized motions, such as when three fish move in parallel and one fish moves in the opposite direction, (the only unbalanced  $(2, N)$ -pattern for  $N = 4$ ). For the  $n = 1$  histogram, the single peak near zero provides the strongest evidence for local synchronization behavior. For both eight-fish data sets, the  $n = N - 1$  scaled potential histograms have a single peak at unity, which is

consistent with the milling behavior and indicates that the group center of mass is predominantly fixed. Although each  $n = 1$  histogram has a single peak as well, the mean is not at zero. Nonetheless, evidence for local synchronization is provided by the histogram of the difference between the values of the scaled potential for  $n = N - 1$  and  $n = 1$ . The difference histogram is nearly always positive, which implies that the entire school is less synchronized than neighboring fish. The result that both the eight-fish data sets contain evidence for local synchronization suggests that the orientation component of the individual fish behaviors may be similar even if the group behavior is different.

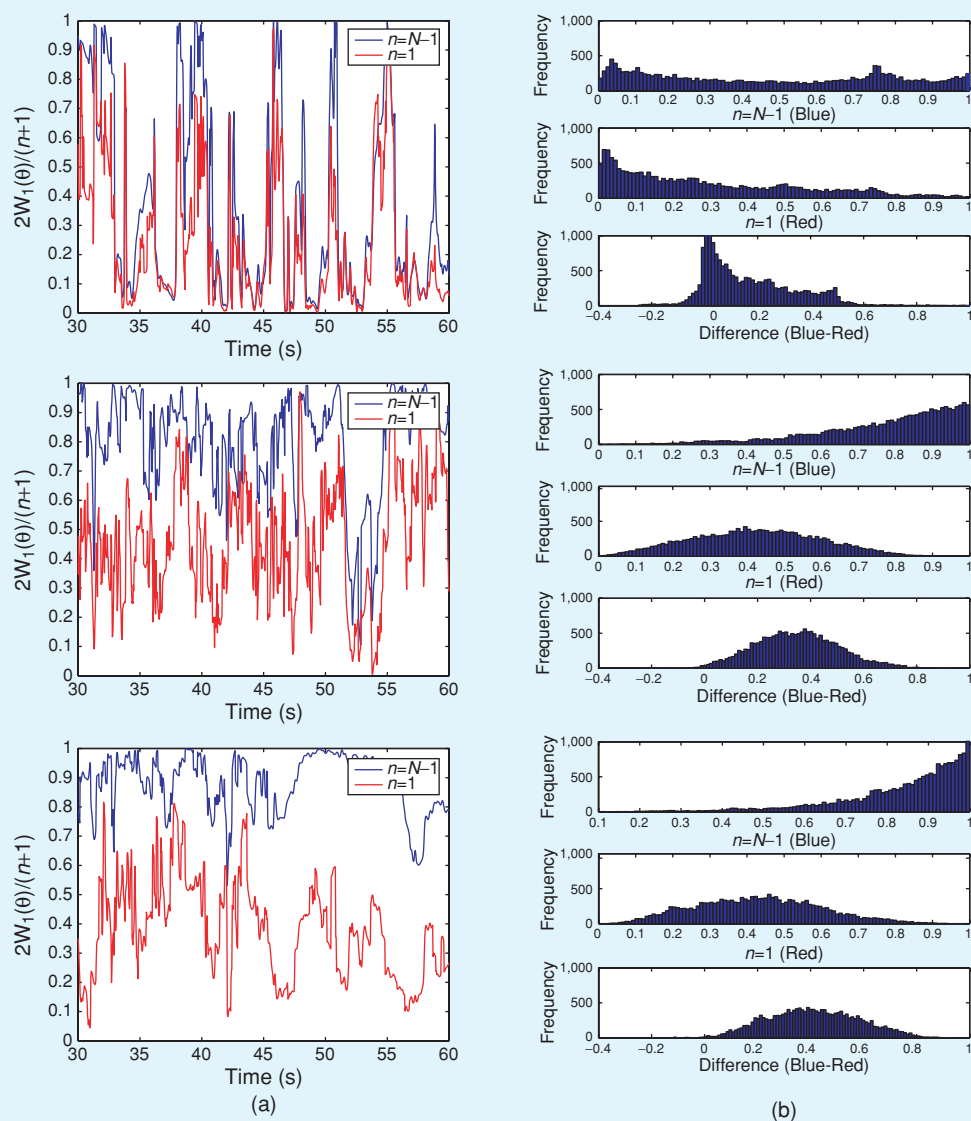


**FIGURE S3** The value of the Laplacian phase potential  $W_1(\theta)$  for fish-schooling data using the directed graph generated by the  $n$  nearest neighbors of each fish. (a) The scaled potentials  $W_1^{\text{blue}} \triangleq 2/(n+1)W_1(\theta)|_{n=N-1}$  and  $W_1^{\text{red}} \triangleq 2/(n+1)W_1(\theta)|_{n=1}$  are shown for a representative 30-s period starting at  $t = 30$  s. (b) Histograms of  $W_1^{\text{blue}}$ ,  $W_1^{\text{red}}$ , and  $W_1^{\text{blue}} - W_1^{\text{red}}$  are shown for: (top row) four-fish experiment; (middle row) tight-milling eight-fish experiment; and (bottom row) diffuse-milling eight-fish experiment.

arrangement satisfies  $p_\theta = 0$ . Differentiating (4) with respect to time, using (1) and comparing to (7), we observe that  $p_\theta$  is equal to the velocity  $\dot{R}$  of the center of mass of the particles, which is proportional to the average linear momentum of the group. The magnitude of the phase order parameter is thus the speed of the center of mass. Therefore, each balanced phase arrangement corresponds to particle motion with a fixed center of mass.

### Controlling Linear Momentum

Controlling the linear momentum of the collective is equivalent to controlling the magnitude  $|p_\theta|$  of the phase order parameter. Consider the rotationally invariant phase potential

$$U_1(\boldsymbol{\theta}) \triangleq \frac{N}{2} |p_\theta|^2, \quad (8)$$

which is maximized by synchronized phase arrangements and minimized by balanced phase arrangements. The gradient of  $U_1(\boldsymbol{\theta})$  is given by

$$\frac{\partial U_1}{\partial \theta_k} = \langle ie^{i\theta_k}, p_\theta \rangle, \quad k = 1, \dots, N.$$

Consider the Taylor series expansion of  $U_1(\boldsymbol{\theta})$  about  $\theta_0 \mathbf{1}$ , where  $\theta_0$  is an arbitrary phase. Since the potential  $U_1(\boldsymbol{\theta})$  is rotationally invariant, it follows that the Taylor series is exactly  $U(\boldsymbol{\theta} + \theta_0 \mathbf{1}) = U(\boldsymbol{\theta})$ . In particular, the first-order term is

## Collaborative Engineering and Biological Analysis

Investigation of collective motion represents an overlap of interests between engineers and biologists who are motivated by different scientific questions. To engineers, the study of biological aggregations is one of many areas in which organisms confront design problems that have close engineering analogs. These organisms may have evolved highly effective solutions that provide performance benchmarks and inspiration, if not actual blueprints, for engineers tasked with coordinating large systems of interacting agents. To biologists, collective motion or, more generally, social response to neighbors, is ubiquitous, ranging from quorum sensing in bacteria to schooling in fish. Yet, establishing mechanistic relationships between realistic individual behaviors and their group characteristics, or distinguishing those characteristics of groups that are the primary benefits of natural selection from those that are incidental or even disadvantageous, remain open problems. The results in this article illustrate a profitable dialogue between biologists, whose observations help motivate novel analytical directions, and engineers, whose mathematical formalisms suggest new and insightful ways of interpreting biological data as measured against idealized but understandable models.

An example of how this conversation can lead to fundamental insights is in the area of scalability. Engineers designing controls for coordinated  $N$ -member groups face the impracticality of information exchange among members as  $N$  gets large. Very large social groups abound in nature; these organisms appear to have solved the problem. However, in nearly all of the biologically inspired simulations of collective motion, large groups lack robustness and tend to fragment easily into smaller groups unless they also contain explicit mechanisms, such as a finite spatial domain or common directional preferences, that suppress the tendency. This difference between theory and observation suggests that critical elements, perhaps intelligent processing of limited sensory data, are missing in our current understanding of collective control algorithms. Understanding this intelligent processing, or per-

haps determining there is no such intelligence, may supply key biomimetic insights for engineers and mechanistic individual-to-group dynamics for biologists.

Analysis of collective behavior is potentially useful in at least two directions. First, these results provide a starting point for the reverse engineering of algorithms from observed trajectories. Biologists' abilities to infer underlying behavior from movement observations has been far more limited, and far more limiting, than their abilities to simulate movement from hypothetical behavioral algorithms. As suggested by the analysis of fish trajectories (see "Analysis of Fish Data"), any analytical infrastructure that permits bidirectional inferences, that is, movement from algorithm and algorithm from movement, is a big step forward, even if the underlying models are simplified compared to real biological behaviors.

Second, the analysis of directed interaction graphs in PCOD promises an explicit link between control theory and the distance-mediated attraction, repulsion, and alignment neighborhoods that are the basis of most social grouping simulations. One interpretation of these results is a biological hypothesis that the dynamics within a fish school continually tend toward locally stable ordered states but are continually perturbed by surrounding neighborhoods of individuals with distinct and possibly incompatible ordered states. If so, the analysis suggests explicit and general predictions of what those states' characteristics must be, and how the balance between stability and perturbation may be statistically reflected in movement data. Biological grouping simulations have long suffered from a lack of generality, with no way of knowing whether simulation results reflect fundamental characteristics of coordinated groups or only idiosyncratic ways of oversimplifying very complex processes. Analytical results that tie general provable results to reasonable biological models promise to move the coordinated group discussion between engineers and biologists toward general necessary and sufficient conditions for attaining specific group properties.

$$\mathbf{1}^T \frac{\partial U_1}{\partial \theta} = \sum_{k=1}^N \langle ie^{i\theta_k}, p_\theta \rangle = N \langle ip_\theta, p_\theta \rangle = 0,$$

which shows that the gradient  $(\partial U_1)/(\partial \theta)$  of  $U_1(\theta)$  is indeed orthogonal to  $\mathbf{1}$ . We use this fact below.

The global maximizers and global minimizers of the potential  $U_1(\theta)$  represent synchronized and balanced phase configurations. A candidate orientation control  $u_k^{\text{ori}}$  that extremizes the value of the potential along solutions of the closed-loop phase model (6) is the gradient of  $U_1(\theta)$  multiplied by the nonzero gain  $-K_1$ , where the minus sign is consistent with the coupled-phase oscillator literature [5]. The candidate control is

$$u_k^{\text{ori}} = -K_1 \langle ie^{i\theta_k}, p_\theta \rangle, \quad k = 1, \dots, N. \quad (9)$$

For the control (9), it follows that

$$\dot{U}_1(\theta) = \frac{\partial U_1}{\partial \theta} \dot{\theta} = -K_1 \sum_{k=1}^N \langle ie^{i\theta_k}, p_\theta \rangle^2,$$

and thus the potential  $U_1(\theta)$  evolves monotonically along solutions of (6).

The phase model (6) with the gradient control (9) is equivalent to

$$\dot{\theta}_k = \omega_0 + \frac{K_1}{N} \sum_{j=1}^N \sin \theta_{kj}. \quad (10)$$

For  $K_1 < 0$ , the system (10) is a simplified version [23] of the Kuramoto model, which is a general model of oscillator synchronization and collective behavior [24]. The oscillators in (10) have identical natural frequencies  $\omega_0$ , whereas, in the Kuramoto model, the oscillators have different natural frequencies. For  $K_1 > 0$ , the system (10) stabilizes balanced phase arrangements. Lyapunov analysis provides the following stability result on all-to-all orientation control given in [25].

### Theorem 1

For the gradient control (9), all of the solutions of the phase model (6) converge to the critical set of  $U_1(\theta)$ , which is the set of all points where the gradient of  $U_1(\theta)$  is zero. If  $K_1 < 0$ , then all of the synchronized phase arrangements are asymptotically stable and all of the remaining equilibria are unstable. If  $K_1 > 0$ , then the balanced equilibria for which  $p_\theta = 0$  are asymptotically stable and all of the remaining equilibria are unstable.

All of the points in the critical set of  $U_1(\theta)$  other than the synchronized and balanced phase arrangements are saddle points. These stationary points satisfy  $\sin \theta_{kj} = 0$  for all  $j, k \in \{1, \dots, N\}$ , which means that these points are equilibria of (6) with the control (9). For example, consider the set of stationary points with  $M < N$  phases equal to  $\theta_0$

and  $N - M$  phases equal to  $\theta_0 + \pi$ . These phase arrangements, called *unbalanced (2, N)-patterns* if  $M \neq N/2$ , are unstable equilibria; they look like two unequally sized clusters of particles on opposite sides of the unit circle.

The particle model (1), (2) with the gradient control (9) gives rise to four distinct types of motion, shown in Figure 1. In particular, for  $\omega_0 = 0$ , the particles move along straight trajectories, while, for  $\omega_0 \neq 0$ , the particles move around circles. In either case, if  $K_1 < 0$ , then the phases are synchronized; if  $K_1 > 0$ , then the center of mass of the particles is fixed. The case  $\omega_0 = 0$  and  $K_1 < 0$ , which is an example of a parallel formation, is the only relative equilibrium shown in Figure 1. Later, we present spacing controls that stabilize circular formations, but first we extend the phase model to systems with limited interaction.

## LAPLACIAN QUADRATIC FORMS

Implicit in the gradient control (9) is the assumption that each particle computes its control using its phase relative to every other particle. In this section, we extend the orientation control (9) to scenarios in which interaction is limited. The orientation interaction network is a directed graph that describes which relative phases are available to each particle for feedback. We also consider spacing controls constrained by a spacing interaction network. We describe here and in the next section a methodology for stabilizing the collective motion of the phase and particle models with limited interaction.

We describe an interaction network by a directed graph  $G$ . Let  $L$  be the Laplacian matrix of  $G$  (see "A Tutorial on Graph Theory"). Let  $\langle \mathbf{x}, \mathbf{y} \rangle \triangleq \sum_{j=1}^N \langle x_j, y_j \rangle$ , where  $\mathbf{x} \triangleq (x_1, \dots, x_N)^T \in \mathbb{C}^N$  and  $\mathbf{y} \triangleq (y_1, \dots, y_N)^T \in \mathbb{C}^N$ . Associated with  $L$  is the Laplacian quadratic form

$$Q_L(\mathbf{x}) \triangleq \frac{1}{2N} \langle \mathbf{x}, L\mathbf{x} \rangle. \quad (11)$$

If  $G$  is undirected, then  $L = BB^T$  (see "A Tutorial on Graph Theory"), and the quadratic form (11) is proportional to the total length of graph edges, that is,

$$Q_L(\mathbf{x}) = \frac{1}{2N} \sum_{(j,k) \in E} |x_j - x_k|^2,$$

where  $E$  is the set of edges of  $G$  (see "A Tutorial on Graph Theory"). If  $G$  is undirected and connected, then  $Q_L(\mathbf{x}) = 0$  if and only if  $\mathbf{x} \in \text{span}\{\mathbf{1}\}$ , while  $Q_L(\mathbf{x}) > 0$  otherwise [17].

### Laplacian Phase Potentials

Consider the Laplacian quadratic form

$$W_1(\theta) \triangleq Q_L(e^{i\theta}) = \frac{1}{2N} \langle e^{i\theta}, L e^{i\theta} \rangle, \quad (12)$$

where  $e^{i\theta} \triangleq (e^{i\theta_1}, \dots, e^{i\theta_N})^T$ . The Laplacian quadratic form (12) is called a Laplacian phase potential [26] since it

generalizes the phase potential  $U_1(\theta)$  defined in (8) for all-to-all particle interaction. If  $G$  is complete (see “A Tutorial on Graph Theory”), then

$$W_1(\theta) = \frac{N}{2} - U_1(\theta), \quad (13)$$

and  $W_1(\theta)$  has the same stationary points as  $U_1(\theta)$ . If  $G$  is strongly connected (see “A Tutorial on Graph Theory”), then  $W_1(\theta) = 0$  if and only if  $\theta$  is synchronized; otherwise,  $W_1(\theta) > 0$ . To see this, we compute

$$\begin{aligned} W_1(\theta) &= \frac{1}{2N} \sum_{k=1}^N \langle e^{i\theta_k}, L_k e^{i\theta} \rangle \\ &= \frac{1}{2N} \sum_{k=1}^N \left( d_k - \underbrace{\sum_{j \in \mathcal{N}_k} \langle e^{i\theta_k}, e^{i\theta_j} \rangle}_{\leq d_k} \right) \geq 0, \end{aligned}$$

where  $d_k$  is the degree of node  $k$  and  $\mathcal{N}_k$  is the set of neighbors of node  $k$  (see “A Tutorial on Graph Theory”). If  $G$  is not strongly connected, then  $W_1(\theta)$  is zero if and only if the phases within each strongly connected subgraph of  $G$  are synchronized; otherwise,  $W_1(\theta)$  is positive.

### Laplacian Phase Control

Assuming now that  $G$  is undirected, the gradient of  $W_1(\theta)$  is

$$\frac{\partial W_1}{\partial \theta_k} = \frac{1}{2N} \langle i e^{i\theta_k}, (L + L^T)_k e^{i\theta} \rangle = \frac{1}{N} \langle i e^{i\theta_k}, L_k e^{i\theta} \rangle,$$

where  $L_k$  denotes the  $k$ th row of the Laplacian matrix. In the phase model (6), choosing the gradient control

$$u_k^{\text{ori}} = \frac{K_1}{N} \langle i e^{i\theta_k}, L_k e^{i\theta} \rangle, \quad k = 1, \dots, N, \quad (14)$$

with  $K_1 \neq 0$ , guarantees that the potential  $W_1(\theta)$  evolves monotonically, since

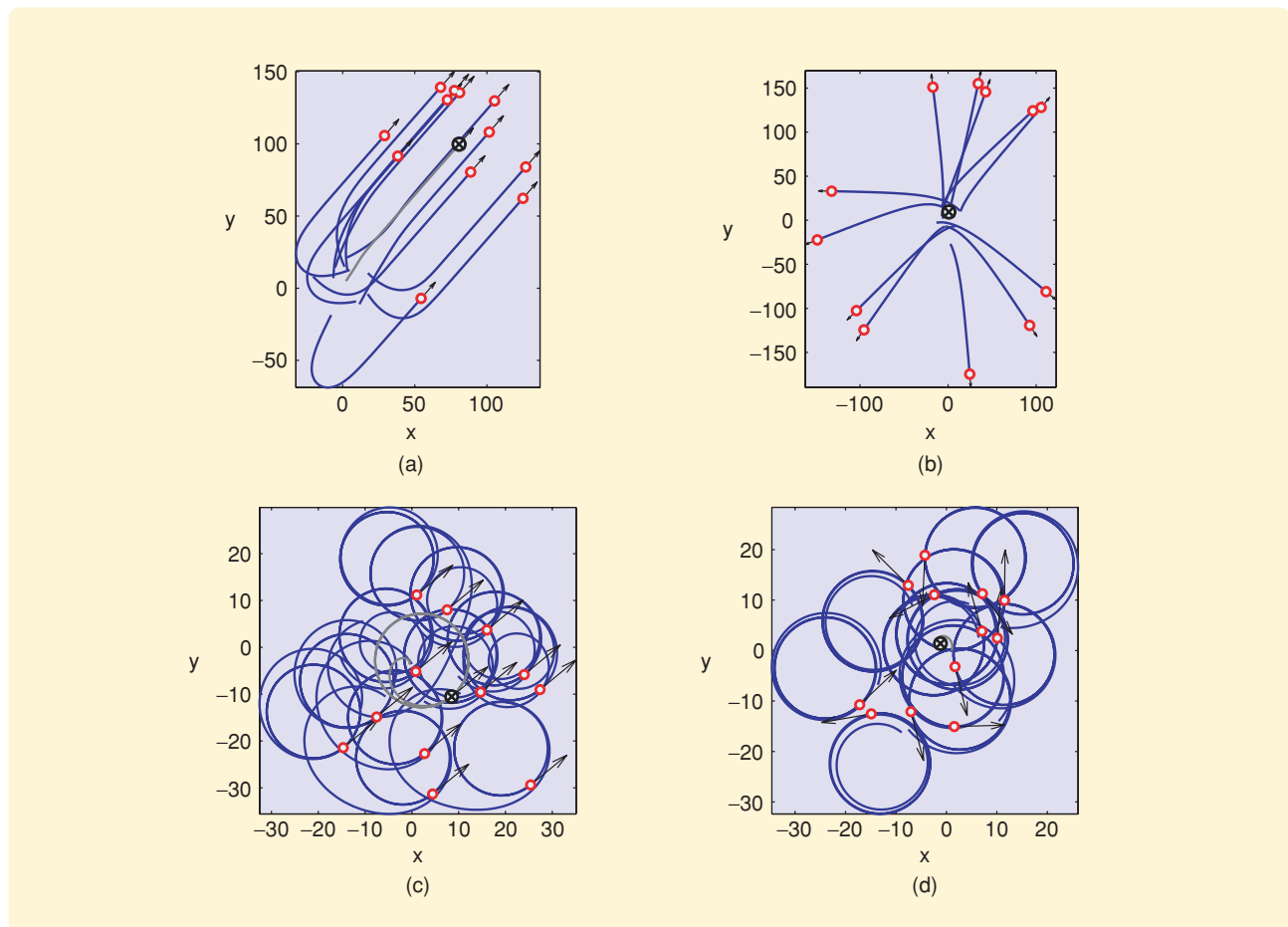


**FIGURE 1** Four types of collective motion obtained with the orientation control (9) and  $N = 12$ . The position  $r_k$  of particle  $k \in \{1, \dots, 12\}$  is a red circle, and the velocity  $e^{i\theta_k}$  is a black arrow. The center of mass  $R$  is the black circle marked by an  $\mathbf{x}$ , and the center of mass velocity  $\dot{R} = p_\theta$  is a black arrow. (a)  $\omega_0 = 0$  and  $K_1 < 0$ . The phases are synchronized, and the particles travel in a parallel formation. (b)  $\omega_0 = 0$  and  $K_1 > 0$ . The phases are balanced, and the center of mass is fixed as the particles travel off along straight lines. (c)  $\omega_0 \neq 0$  and  $K_1 < 0$ . The phases are synchronized as each particle travels around a circle. (d)  $\omega_0 \neq 0$  and  $K_1 > 0$ . The phases are balanced, and the center of mass is fixed as the particles travel around (different) circles. Only (a) is a relative equilibrium of the model (1), (2).

$$\dot{W}_1(\boldsymbol{\theta}) = \frac{\partial W_1}{\partial \boldsymbol{\theta}} \dot{\boldsymbol{\theta}} = \frac{K_1}{N^2} \sum_{k=1}^N \langle ie^{i\theta_k}, L_k e^{i\boldsymbol{\theta}} \rangle^2.$$

The phase model (6) with the gradient control (14) is equivalent to

$$\dot{\theta}_k = \omega_0 + \frac{K_1}{N} \sum_{j \in \mathcal{N}_k} \sin \theta_{kj}, \quad (15)$$

where  $K_1 \neq 0$ . By comparison with (10), we observe that the system (15) with  $K_1 < 0$  is a simplified Kuramoto model of identical coupled-phase oscillators with limited interaction. Equation (15) also demonstrates that (14) is a shape control since it depends only on the relative phases.

The invariance principle shows that the phase model under the control (14) converges to the largest invariant set for which  $\dot{W}_1(\boldsymbol{\theta}) = 0$ , which corresponds to the condition

$$\langle ie^{i\theta_k}, L_k e^{i\boldsymbol{\theta}} \rangle = 0, \quad k = 1, \dots, N. \quad (16)$$

The vector  $e^{i\boldsymbol{\theta}}$  satisfies (16) if and only if  $\boldsymbol{\theta}$  is a stationary point of the phase potential  $W_1(\boldsymbol{\theta})$  [27]. For example, if  $e^{i\boldsymbol{\theta}}$  is an eigenvector of  $L$ , then  $\boldsymbol{\theta}$  is a stationary point of  $W_1(\boldsymbol{\theta})$

and an equilibrium of (6). The set of stationary points that are synchronized corresponds to the eigenvector  $\mathbf{1}$ , that is,  $\theta_k = \theta_j$  for all pairs  $k$  and  $j$ . This set, whose elements are global minimizers of the phase potential, is not empty for any connected graph. The set of balanced stationary points satisfies  $\mathbf{1}^T e^{i\boldsymbol{\theta}} = 0$ . A sufficient condition for the existence of a balanced stationary point is that  $G$  is circulant, that is, the Laplacian is a circulant matrix.

If  $G$  is circulant, then  $L$  is diagonalized by the discrete Fourier transform matrix  $F \triangleq [f_{km}] \in \mathbb{C}^{N \times N}$ , where  $f_{km} = 1/\sqrt{N} e^{i(2\pi/N)(m-1)(k-1)}$  (see "A Tutorial on Graph Theory"). The columns of  $F$  are (normalized) eigenvectors of  $L$ . Therefore, if  $e^{i\boldsymbol{\theta}}$  is an eigenvector of a circulant Laplacian other than  $\mathbf{1}$ , then the phasors  $e^{i\theta_k}$  form a symmetric pattern on the unit circle. In the case of the cyclic graph  $C_N$ , the edges of the graph form a generalized regular polygon [28]. The eigenvectors and corresponding eigenvalues of the Laplacian of  $C^N$  are shown in Figure 2.

## STABILIZING SPATIAL PATTERNS

We now summarize an approach to stabilizing spatial patterns using PCOD with Laplacian-based controls. A circular

## A Tutorial on Graph Theory

Consider the directed graph  $G = (\mathcal{N}, E)$ , where  $\mathcal{N} \triangleq \{1, \dots, N\}$  is a set of nodes and  $E \subset \mathcal{N} \times \mathcal{N}$  is a set of directed edges. In this setting, node  $k$  of  $G$  corresponds to particle  $k$  and the ordered pair  $(j, k) \in E$  corresponds to information flow from particle  $j$  to  $k$ . Assume there are no self-loops, which means  $(k, k) \notin E$  for all  $k = 1, \dots, N$ . If  $(j, k) \in E$ , then  $j$  is a neighbor of  $k$ . The set  $\mathcal{N}_k$  contains all of the neighbors of  $k$ ; the cardinality  $d_k$  of  $\mathcal{N}_k$  is the number of neighbors of  $k$ , which is the degree of node  $k$ . If  $j$  is a neighbor of  $k$ , then the (relative) states of particle  $j$  are available for computing control  $u_k$ . In the case that  $j$  is a neighbor of  $k$  if and only if  $k$  is a neighbor of  $j$ , then  $G$  is undirected. If there is a path that obeys edge direction between every pair of distinct nodes, then  $G$  is strongly connected. If  $G$  is undirected and strongly connected, then we say  $G$  is connected.

There are several matrix representations of a directed graph  $G$ . Let  $\mathbf{d} \triangleq (d_1, \dots, d_N)^T \in \mathbb{R}^N$ . The degree matrix  $D$  is the positive-semidefinite matrix  $D \triangleq \text{diag}(\mathbf{d})$ . The adjacency matrix  $A$  is the matrix  $A = [a_{kj}] \in \mathbb{R}^{N \times N}$ , where  $a_{kj} = 1$ , if  $j \in \mathcal{N}_k$ , and  $a_{kj} = 0$ , otherwise. The incidence matrix  $B$  is the matrix  $B = [b_{kf}] \in \mathbb{R}^{N \times e}$ , where each column of  $B$  corresponds to a single edge in  $E$ , where  $e$  is the cardinality of  $E$ . Let column  $f \in \{1, \dots, e\}$  correspond to edge  $(j, k) \in E$ ; in this case,  $b_{kf} = 1 = -b_{jf}$  and all of the remaining entries of column  $f$  are zero. The Laplacian matrix  $L$  is defined by  $L \triangleq D - A$ . It can be shown using the Geršgorin disc theorem [35, p. 344] that all of

the eigenvalues of  $L$  have nonnegative real part. Furthermore, if  $G$  is undirected, then the Laplacian matrix of  $G$  is symmetric and satisfies  $L = BB^T$ , which means that  $L$  is positive semidefinite.

We describe the Laplacians of two undirected graphs. Let  $K_N$  denote the complete graph of  $N$  nodes, each with degree  $N - 1$ . Let  $C_N$  denote the undirected cyclic graph of  $N$  nodes, which is a connected graph in which each node has degree 2. Both types of graphs are circulant, which means that their Laplacian matrices are circulant and symmetric matrices. Circulant matrices with  $N \geq 2$  columns are completely defined by their first row; each remaining row starts with the last entry of the previous row followed by the first  $N - 1$  entries of the previous row. Let  $L_k$  be the  $k$ th row of the graph Laplacian. For the complete graph, we have  $L_1 \triangleq (N - 1, -1, \dots, -1) \in \mathbb{R}^N$ . For a cyclic graph, we have  $L_1 \triangleq (2, -1, 0, \dots, 0, -1) \in \mathbb{R}^N$ . (See [36] for more examples of undirected circulant graphs.) Circulant graphs are also  $d_0$ -regular, meaning  $\mathbf{d} = d_0 \mathbf{1}$ . We have  $d_0 = N - 1$  for the graph  $K_N$  and  $d_0 = 2$  for the graph  $C_N$ .

By definition,  $L\mathbf{1} = \mathbf{0}$ , which implies that zero is an eigenvalue of  $L$ . If  $G$  is strongly connected, then zero as an eigenvalue of  $L$  has multiplicity one [37]. If  $G$  is undirected, then  $L$  is symmetric and its (normalized) eigenvectors can be chosen to form an orthonormal basis. If  $G$  is undirected, then  $G$  is circulant if  $L$  is symmetric and circulant; in this case, the unitary matrix  $F$ , whose columns are normalized eigenvectors of  $L$ , is the discrete Fourier transform matrix [38].

formation is a relative equilibrium in which all of the particles travel around the same circle. Stabilizing formations on a more general class of closed curves is discussed in [29]. It is shown below how to use a composite potential to isolate symmetric patterns of the particles in a circular formation, where isolate means to create a local basin of attraction that contains no other solutions in shape space. We assume fixed, undirected, and connected graphs for orientation and spacing interactions; extensions to time-varying, directed interactions are given in [7].

### Circular Formations

Let  $\mathbf{c} \triangleq (c_1, \dots, c_N)^T \in \mathbb{C}^N$ , where the circle center  $c_k$  is defined by (3) with  $\omega_0 \neq 0$ . Particles in a circular formation satisfy the algebraic condition  $\mathbf{c} = c_0 \mathbf{1}$ , where  $c_0 \in \mathbb{C}$ . Let  $L$  be the Laplacian of the undirected and connected graph  $G$ . We use the Laplacian quadratic form

$$S(\mathbf{r}, \boldsymbol{\theta}) \triangleq Q_L(\mathbf{c}) = \frac{1}{2N} \langle \mathbf{c}, L\mathbf{c} \rangle \quad (17)$$

to define a spacing potential that is zero in the circular formation and positive otherwise. The potential  $S(\mathbf{r}, \boldsymbol{\theta})$  is positive definite and proper in the reduced space of relative circle centers, which have coordinates  $c_{kj} \triangleq c_k - c_j$ . Differentiating (3) with respect to time along solutions of (1), (2) yields

$$\dot{c}_k = e^{i\theta_k} (1 - \omega_0^{-1} u_k), \quad k = 1, \dots, N. \quad (18)$$

Using (18), the potential (17) evolves along the solutions of the particle model (1), (2) according to

$$\dot{S}(\mathbf{r}, \boldsymbol{\theta}) = \frac{1}{N} \sum_{k=1}^N \langle e^{i\theta_k}, L_k \mathbf{c} \rangle (1 - \omega_0^{-1} u_k). \quad (19)$$

We assume controls of the form (5) with, for the moment,  $u_k^{\text{ori}} = 0$ . Choosing

$$u_k^{\text{spac}} = \omega_0 \frac{K_0}{N} \langle e^{i\theta_k}, L_k \mathbf{c} \rangle, \quad k = 1, \dots, N, \quad (20)$$

where  $K_0 > 0$ , and using (5), (19), and (20), we obtain

$$\dot{S}(\mathbf{r}, \boldsymbol{\theta}) = -\frac{K_0}{N^2} \sum_{k=1}^N \langle e^{i\theta_k}, L_k \mathbf{c} \rangle^2 \leq 0,$$

which guarantees that  $S(\mathbf{r}, \boldsymbol{\theta})$  is nonincreasing. Lyapunov analysis provides the following global stability result for Laplacian circular formation control given by [27].

### Theorem 2

For the control (5) with  $u_k^{\text{ori}} = 0$  and  $u_k^{\text{spac}}$  given in (20), all of the solutions of the particle model (1), (2) converge to the set of circular formations with radius  $|\omega_0|^{-1}$  and direction of rotation determined by the sign of  $\omega_0 \neq 0$ .

By the invariance principle, solutions converge to the largest invariant set for which  $\dot{S}(\mathbf{r}, \boldsymbol{\theta}) = 0$ . In this set,  $\dot{\theta} = \omega_0 \mathbf{1}$  and  $\mathbf{c} = c_0 \mathbf{1}$ . Since the spacing control (20) is a shape control that preserves the rotation and translation symmetries of the particle model, the steady-state position of the center of the circular formation  $c_0 \in \mathbb{C}$  depends only on the initial state of the particles and is fixed. On the other hand, the center of mass of the particles is not necessarily fixed.

### Synchronized and Balanced Circular Formations

We show next how to stabilize the circular formation and, simultaneously, control the speed of the center of mass. Assume for now that the orientation and spacing interaction networks are identical. Consider the composite potential formed by taking a linear combination of the spacing potential  $S(\mathbf{r}, \boldsymbol{\theta})$  and the phase potential  $W_1(\boldsymbol{\theta})$ , given by

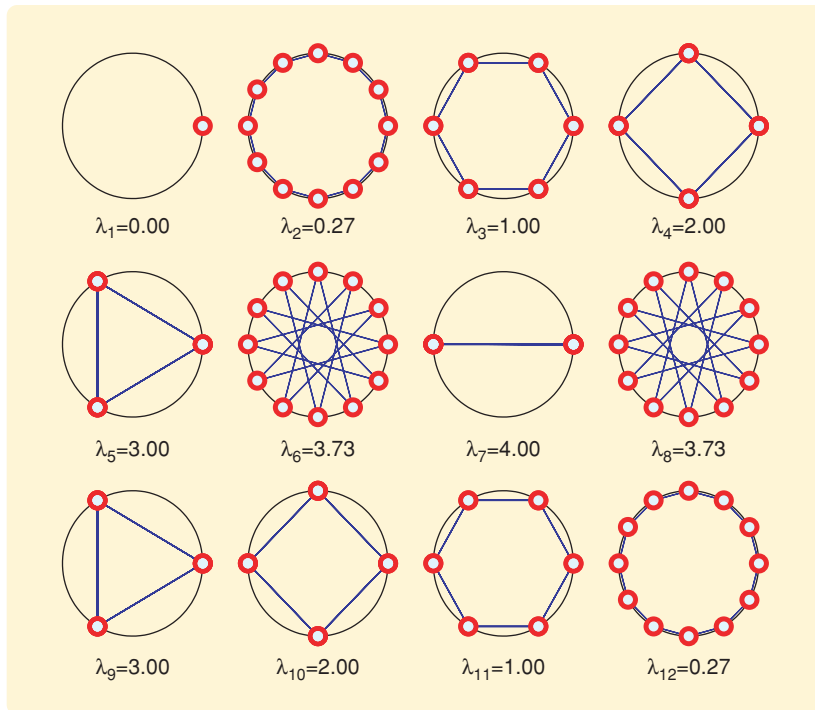


**FIGURE 2** Eigenvectors of the Laplacian  $L$  of the cyclic graph  $C_{12}$ . If  $e^{i\theta}$  is an eigenvector of  $L$ , then  $\theta$  is a stationary point of the Laplacian phase potential (12), and  $\theta$  forms a symmetric pattern on the unit circle. The edges of each graph form generalized regular polygons.

$$V(\mathbf{r}, \boldsymbol{\theta}) \triangleq K_0 S(\mathbf{r}, \boldsymbol{\theta}) + K_1 \omega_0^{-1} W_1(\boldsymbol{\theta}), \quad (21)$$

where  $K_0 > 0$ ,  $K_1 \neq 0$ , and  $\omega_0 \neq 0$ . We simultaneously stabilize the circular formation and the speed of the center of mass by choosing the control (5) with  $u_k^{\text{ori}}$  given by (14) and  $u_k^{\text{spac}}$  given by (20), that is,

$$u_k = \omega_0 + \frac{K_1 - K_0}{N} \langle ie^{i\theta_k}, L_k e^{i\boldsymbol{\theta}} \rangle + \omega_0 \frac{K_0}{N} \langle e^{i\theta_k}, L_k \mathbf{r} \rangle. \quad (22)$$

Taking the time derivative of (21) along the solutions of (1), (2), and using (12), (17) and (22), we obtain

$$\dot{V}(\mathbf{r}, \boldsymbol{\theta}) = -\frac{1}{N^2} \sum_{k=1}^N (K_0 \langle e^{i\theta_k}, L_k \mathbf{c} \rangle + K_1 \omega_0^{-1} \langle ie^{i\theta_k}, L_k e^{i\boldsymbol{\theta}} \rangle)^2 \leq 0.$$

By the invariance principle, solutions converge to the largest invariant set for which  $\dot{V}(\mathbf{r}, \boldsymbol{\theta}) = 0$ . In this set,  $\dot{\boldsymbol{\theta}} = \omega_0 \mathbf{1}$ , which implies that both  $\mathbf{c}$  and  $W_1(\boldsymbol{\theta})$  are constant. Consequently, it can be shown that the set of synchronized circular formations, characterized by  $\mathbf{c} = c_0 \mathbf{1}$  and  $|p_\theta| = 1$ , is locally exponentially stable for  $K_1 < 0$ . If, in addition to being connected,  $G$  is also circulant, then it can be shown that the set of balanced circular formations characterized by  $\mathbf{c} = c_0 \mathbf{1}$  and  $p_\theta = 0$  is asymptotically stable for  $K_1 > 0$  [27]. These spatial patterns are shown in Figure 3 for a cyclic graph. Increasing the gain  $K_1 > 0$  in Figure 3(c) produces the balanced  $(2, N)$ -pattern, which is the unique configuration that maximizes the potential  $W_1(\boldsymbol{\theta})$ .

### Symmetric Circular Formations

Next, we derive phase potentials that isolate symmetric circular formations, which are circular formations in which the phase arrangement is a symmetric pattern. Let the positive integer  $M$  be a divisor of  $N$ . An  $(M, N)$ -pattern is a symmetric arrangement of  $N$  phases consisting of  $M$  clusters uniformly spaced around the unit circle, each with  $N/M$  synchronized phases. For any  $N$ , there exist at least two symmetric patterns, namely, the  $(1, N)$ -pattern, which is the synchronized state, and the  $(N, N)$ -pattern, which is the splay state, characterized by  $N$  phases uniformly spaced around the circle. All of the symmetric patterns other than the synchronized state are balanced.

To characterize  $(M, N)$ -patterns, we generalize the phase order parameter (7) by defining the  $m$ th moment of the phasor distribution as

$$p_{m\theta} \triangleq \frac{1}{mN} \sum_{k=1}^N e^{im\theta_k}, \quad (23)$$

where  $m$  is a positive integer. Symmetric  $(M, N)$ -patterns satisfy  $p_{m\theta} = 0$  for  $m = 1, \dots, M-1$ , which is balancing modulo  $2\pi/m$ , and  $M|p_{M\theta}| = 1$ , which is synchronization modulo  $2\pi/M$  [25].

We stabilize symmetric patterns by designing phase potentials that are minimized by the desired pattern. Consider the Laplacian phase potential

$$W_m(\boldsymbol{\theta}) \triangleq Q_L \left( \frac{1}{m} e^{im\boldsymbol{\theta}} \right) = \frac{1}{2Nm^2} \langle e^{im\boldsymbol{\theta}}, L e^{im\boldsymbol{\theta}} \rangle,$$

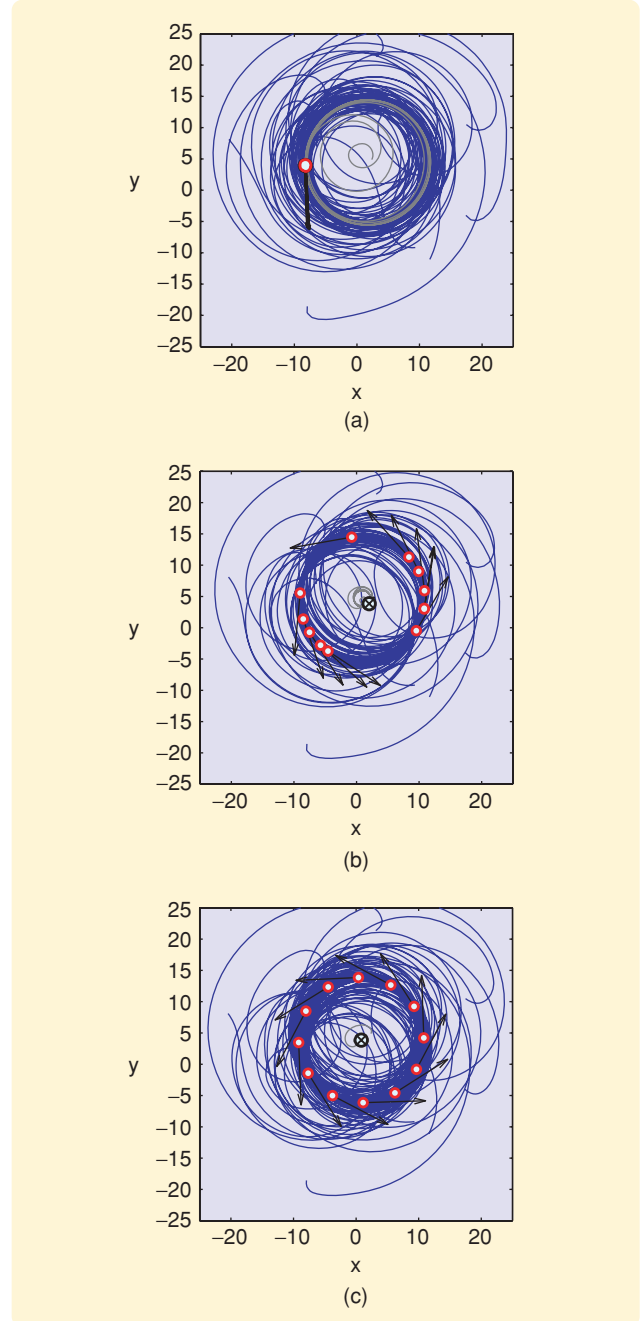


**FIGURE 3** Stabilizing the circular formation with and without orientation control. The spacing and orientation interaction networks are identical, cyclic graphs. Each figure has  $N = 12$ ,  $\omega_0 = 0.1$ , and  $K_0 = N\omega_0$ . (a)  $K_1 < 0$ ; the synchronized circular formation. (b)  $K_1 = 0$ ; an arbitrary circular formation. (c)  $K_1 > 0$ ; the splay circular formation. Increasing the gain  $K_1 > 0$  in (c) produces the balanced  $(2, N)$ -pattern that maximizes the potential  $W_1(\boldsymbol{\theta})$ .

where  $L$  is the Laplacian of the connected, undirected graph  $G$ . The procedure for stabilizing symmetric patterns of particles with limited communication is described in [7]. Here we summarize the results for the complete graph, which represents all-to-all interaction. If  $G$  is complete, then  $W_m(\boldsymbol{\theta}) = (N/2) - U_m(\boldsymbol{\theta})$ , where

$$U_m(\boldsymbol{\theta}) \triangleq \frac{N}{2} |p_{m\theta}|^2 \quad (24)$$

is a natural generalization of the potential  $U_1(\boldsymbol{\theta})$  [25]. The potential  $U_m(\boldsymbol{\theta})$  reaches its minimum when  $p_{m\theta} = 0$  and its maximum when the phase difference between any two phases is an integer multiple of  $2\pi/m$ . All of the remaining stationary points of  $U_m(\boldsymbol{\theta})$  are isolated saddle points [25]. Note that the minimizers of  $U_m(\boldsymbol{\theta})$  are balanced modulo  $2\pi/m$ , while the maximizers of  $U_m(\boldsymbol{\theta})$  are synchronized modulo  $2\pi/m$ .

As before, we combine the circular formation spacing potential with a phase potential to drive the particles to the circular formation in a particular phase arrangement. The composite potential that isolates an  $(M, N)$ -pattern circular formation is given by

$$V^{M,N}(\mathbf{r}) \triangleq K_0 S(\mathbf{r}, \boldsymbol{\theta}) + U^{M,N}(\boldsymbol{\theta}),$$

where  $U^{M,N}(\boldsymbol{\theta})$  is defined by (25) below. The six symmetric patterns for  $N = 12$  are shown in Figure 4. The follow-

ing result for stabilization of symmetric circular formations given in [25] can be proved with Lyapunov analysis.

### Theorem 3

Let the positive integer  $M$  be a divisor of  $N$ . The phase arrangement  $\boldsymbol{\theta} \in \mathbb{T}^N$  is an  $(M, N)$ -pattern if and only if  $\boldsymbol{\theta}$  is a global minimizer of

$$U^{M,N}(\boldsymbol{\theta}) \triangleq \sum_{m=1}^M K_m U_m(\boldsymbol{\theta}), \quad (25)$$

where  $K_m > 0$  for  $m = 1, \dots, M-1$ ,  $K_M < 0$ , and  $U_m(\boldsymbol{\theta})$  is given by (24). Each  $(M, N)$ -pattern circular formation of radius  $|\omega_0|^{-1}$  is an isolated relative equilibrium of the particle model (1), (2) and is exponentially stabilized by the control law (5) with  $u_k^{\text{ori}}$  given by the negative gradient of (25) and  $u_k^{\text{spac}}$  given by (20).

### Symmetry Breaking

Up to now, we have used shape controls to preserve the symmetries that render the particle model invariant to rigid rotation and translation of all of the particles. For a control law that is not a shape control, the closed-loop particle model may not be invariant to rigid rotation or translation of all of the particles. Such a control, which is motivated by application to sensor networks, is said to break the rotation or translation symmetry. In the case of all-to-all interaction, the particle model is also invariant to permutations of particle indices. The engineering design of interaction networks that break the permutation symmetry is described in [7].

We break the rotational symmetry by adding a reference phase  $\theta_0$  that has dynamics  $\dot{\theta}_0 = \omega_0$ . In the closed-loop particle (or phase) model with orientation control (14), we couple at least one particle to the reference phase. Without loss of generality, we couple the  $N$ th particle to the reference phase. The potential  $W_1(\boldsymbol{\theta}) + 1 - \cos(\theta_0 - \theta_N)$  is minimized by  $\theta_k = \theta_0$  for all  $k \in \{1, \dots, N\}$ . When  $\omega_0 \neq 0$ , this configuration corresponds to a circular formation in which every particle's phase is synchronized with the reference phase. When  $\omega_0 = 0$ , this configuration corresponds to parallel motion in the direction of the reference phase  $\theta_0$ . Using this procedure, the collective tracks a piecewise-linear reference trajectory shown in Figure 5 [25].

Similarly, suppose that the position of a reference beacon in

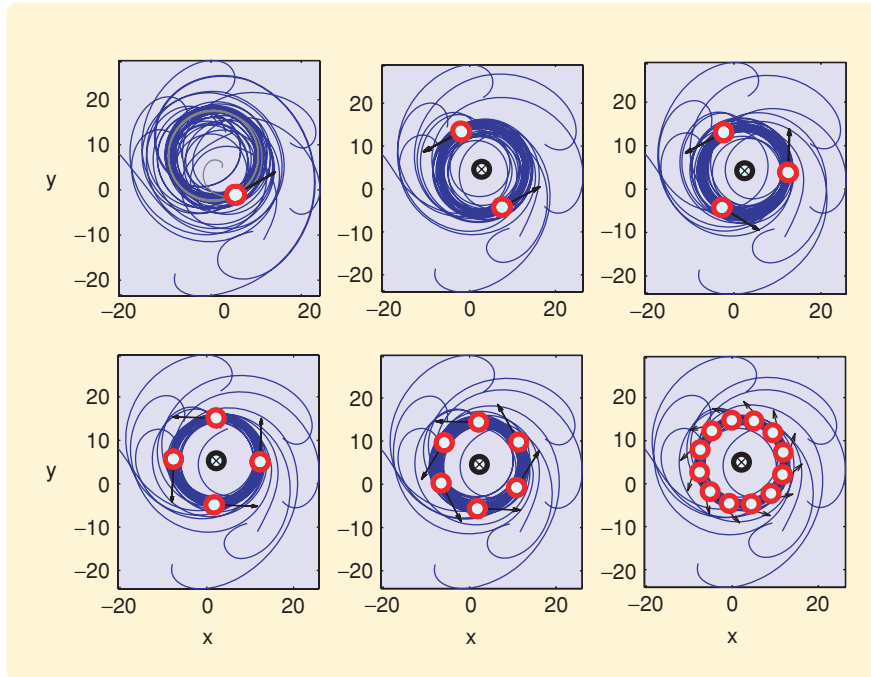


**FIGURE 4** Symmetric circular formations with all-to-all interaction and  $N = 12$ . The patterns correspond to  $M = 1, 2, 3, 4, 6,$  and  $12$  evenly spaced clusters with  $\omega_0 = K_0 = 0.1$ ,  $K_m > 0$  for  $m = 1, \dots, M-1$ , and  $K_M < 0$ . The top left is the synchronized circular formation, while the bottom right is the splay circular formation.

**We describe a framework called particles with coupled oscillator dynamics,  
which extends coupled oscillator dynamics to include spatial dynamics.**

the complex plane is denoted by  $c_0 \in \mathbb{C}$ . Then the quadratic form  $1/(2N)\|\mathbf{c} - c_0\mathbf{1}\|^2$  is zero if and only if  $c_k = c_0$  for all  $k \in \{1, \dots, N\}$ , which corresponds to each particle traveling around a circle that is centered at the beacon  $c_0$ . The spacing control that forces this potential to monotonically decrease fixes the center of the circular formation to  $c_0$ . We illustrate this procedure in Figure 6 for the particle model with a constant-drift vector field, that is,  $\dot{r}_k = e^{i\theta_k} + f_k$ , where  $f_k \in \mathbb{C}$ . If each particle is assigned a different beacon, we obtain a form of collective motion that is well suited for broad area coverage by a mobile sensor network [8].

### BIOLOGICAL COLLECTIVES: MODEL, SIMULATIONS, AND OBSERVATIONS

In this section, we use PCOD to model schooling behavior in fish, and show that, under slow variation of a parameter related to fish interaction, the collective exhibits sharp transitions between different types of motion. We also use PCOD to analyze real fish trajectory data (see “Analysis of Fish Data”). Here, we describe a behavior model in which the fish move at constant speed following several steering behaviors; see, for example, [19]. Although we study fish in this article, the behavior model also applies to other grouping organisms.

We assume that the response of each fish to its neighbors depends on its relative position and relative phase projected onto a horizontal plane. The perceptual range, which defines the sensory neighborhood of each fish, is represented by the union of three concentric zones. These zones correspond to three possible responses to a sensed fish, namely, repulsion, orientation, and attraction. We also assume that the directed sensing capability of each fish generates a blind spot directly behind it. We illustrate these zones and the corresponding behavior in Figure 7.

#### Collective Behavior Model

As in the simple particle model, let  $r_k \in \mathbb{C}$  and  $\theta_k \in S^1$  be the position and direction of motion of the  $k$ th fish. Let  $\rho_{\text{rep}}$ ,  $\rho_{\text{ori}}$ , and  $\rho_{\text{att}}$  define the zone boundaries in Figure 7. For example, the orientation zone of the  $k$ th fish is contained in the annulus  $\{r \mid \rho_{\text{rep}} \leq |r - r_k| \leq \rho_{\text{ori}}\}$ . The angular width of the blind spot behind the  $k$ th fish is denoted by  $\alpha_k$ . In this setting, we use graph theory to describe the time-varying interaction networks generated by the three zones. Note that the interaction networks may be directed due to the blind spot and may be unconnected due to the limited size of the perceptual range. In the case of a

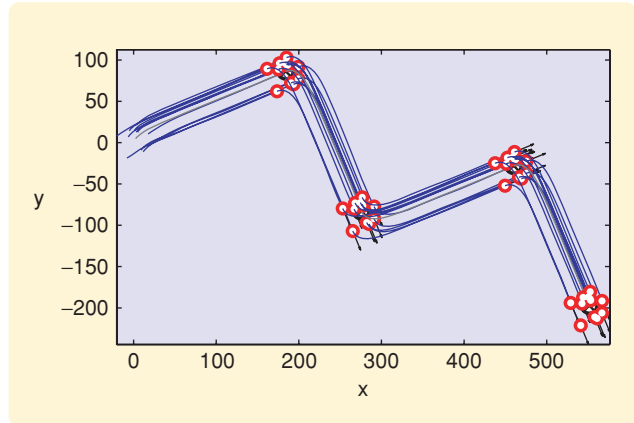


**FIGURE 5** Collective trajectory tracking in a parallel formation with  $N = 12$ . The control (14) tracks a piecewise-linear reference trajectory with  $N = 12$ ,  $\omega_0 = 0$ , and  $K_1 < 0$ . The sequence of reference phases is  $\pi/8, -3\pi/8, \pi/8$ , and  $-3\pi/8$ .

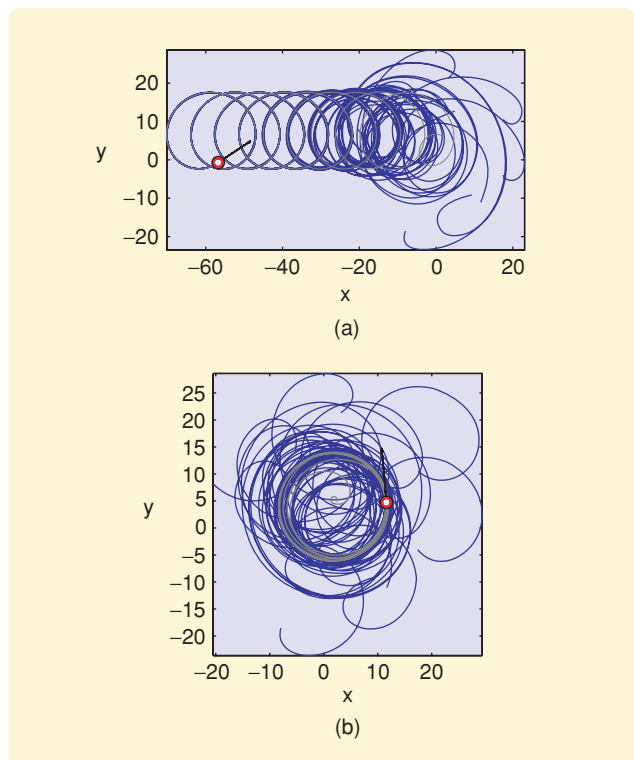


**FIGURE 6** Stabilizing the synchronized circular formation in a drift vector field  $f_k$ . The parameter values are  $f_k = -0.1$ ,  $N = 12$ ,  $\omega_0 = K_0 = 0.1$ , and  $K_1 > 0$ . (a) No beacon; the collective travels in the direction of the vector field. (b) Beacon at  $c_0 = 10$ ; the collective orbits a fixed center.

**In addition to its application as a design methodology, PCOD can also be used to model and analyze schooling behavior in fish.**

directed network, the edges represent information flow originating from the sensed fish. We denote by  $\mathcal{N}_k^{(l)}$  the set of fish sensed by the  $k$ th fish in zone  $l \in \{\text{rep}, \text{ori}, \text{att}\}$ . We also make the simplifying assumptions that the fish have unit mass, travel at unit speed, and maneuver only by steering.

Let  $q = 0, 1, 2, \dots$  denote the  $q$ th time step of a discrete-time model. For  $k = 1, \dots, N$ , the fish model is

$$\begin{aligned} r_k(q+1) &= r_k(q) + e^{i\theta_k(q)}, \\ \theta_k(q+1) &= \theta_k(q) + Tu_k(q), \end{aligned} \quad (26)$$

where  $T \ll 1$  is the fish response latency and  $u_k(q)$  is the steering behavior. Observe that the fish model (26) is the forward Euler method approximation to the continuous-time particle model (1), (2). Given concentric zones of repulsion, orientation, and attraction, the corresponding desired behavior vector fields for fish  $k = 1, \dots, N$  are given by [19]

$$\begin{aligned} \mathbf{v}_k^{\text{rep}}(q) &= - \sum_{j \in \mathcal{N}_k^{\text{rep}}(q)} \hat{r}_{kj}(q), \\ \mathbf{v}_k^{\text{ori}}(q) &= e^{i\theta_k(q)} + \sum_{j \in \mathcal{N}_k^{\text{ori}}(q)} e^{i\theta_j(q)}, \\ \mathbf{v}_k^{\text{att}}(q) &= \sum_{j \in \mathcal{N}_k^{\text{att}}(q)} \hat{r}_{kj}(q), \end{aligned}$$

where  $\hat{r}_{kj}(q) \triangleq (r_{kj}(q)/|r_{kj}(q)|)$  and  $\mathcal{N}_k^{(l)}(q)$  are the neighbors of fish  $k$  in zone  $l$  at time  $q$ . We represent additional motion

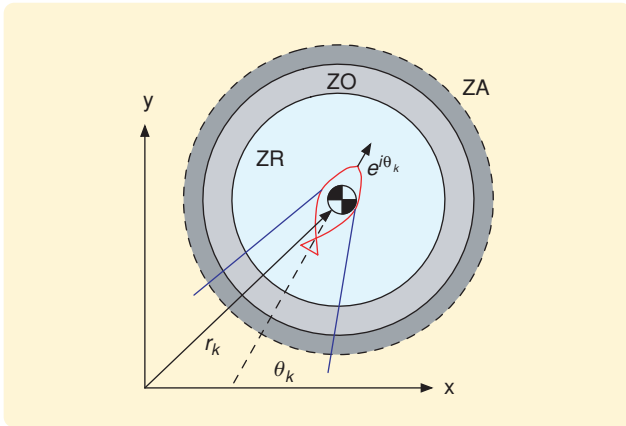


**FIGURE 7** Concentric perceptual zones in the fish model (26). These zones include the attraction zone (ZA), orientation zone (ZO), and repulsion zone (ZR) [19]. The blind spot, which is behind the fish between the blue lines, has angular width  $\alpha_k$ .

that is uncoupled from the remaining fish by a possibly random behavior term  $\omega_k(q)$ . The steering behavior is

$$\begin{aligned} u_k(q) &= \omega_k(q) + \langle ie^{i\theta_k}(q), K_{\text{rep}} \mathbf{v}_k^{\text{rep}}(q) \\ &\quad + K_{\text{ori}} \mathbf{v}_k^{\text{ori}}(q) + K_{\text{att}} \mathbf{v}_k^{\text{att}}(q) \rangle, \end{aligned} \quad (27)$$

where the gains satisfy  $K_{\text{rep}} \gg K_{\text{ori}} > 0$  and  $K_{\text{rep}} \gg K_{\text{att}} > 0$ . Next, we express these behaviors using the graph Laplacian and relate them to the particle-model steering controls.

We can write the steering behavior (27) in terms of the degree  $D^{(l)}$ , adjacency  $A^{(l)}$ , and Laplacian  $L^{(l)}$  matrices of the directed graph in zone  $l$ . Dropping the  $q$  notation, if the repulsion zone of the  $k$ th fish is empty, we approximate (27) as

$$u_k = \omega_k - K_{\text{ori}} \langle ie^{i\theta_k}, L_k^{\text{ori}} e^{i\theta} \rangle + K_{\text{att}} \langle ie^{i\theta_k}, L_k^{\text{att}} \mathbf{r} \rangle. \quad (28)$$

Note the resemblance between the steering behavior (28) and the circular control (22). In place of the constant natural frequency  $\omega_0$ , the fish behavior contains the variable turning rate  $\omega_k$ . The alignment terms are identical for  $K_1 - K_0 = -K_{\text{ori}}N < 0$ , which represents a behavior that seeks to align the fish velocities. The spacing terms differ only by a factor of  $i$ , which is a consequence of their differing motivations as described next.

Let  $\tilde{r}_k \triangleq d_k^{-1} L_k^{(l)} \mathbf{r} = r_k - d_k^{-1} \sum_{j \in \mathcal{N}_k^{(l)}} r_j$  be the vector from the center of mass of the neighbors of fish  $k$  in zone  $l$  to the position of fish  $k$ . The circular control of the fish model locally stabilizes motion of the  $k$ th fish perpendicular to  $\tilde{r}_k$ . In contrast, both the attraction and repulsion behaviors in the fish model stabilize motion parallel to  $\tilde{r}_k$ ; this motion is appropriate for aggregation with collision avoidance.

Although we focus on circular formations in the next subsection, we do not claim that the circular motion control is an accurate model of fish behavior. Rather, stabilizing the circular formation is an example of activity consensus, that is, individuals moving around together. The circular motion activity keeps the center of mass of the particle group confined to a fixed ball of radius  $|\omega_0|^{-1}$ . Stabilizing parallel motion is another form of activity consensus in which individuals move off together.

### Bifurcations of Collective Motion

Simulation studies suggest that fish group behavior can be influenced merely by selecting the number of influential neighbors and not by changing the behavior rule

itself [22]. In this subsection, we study qualitative changes in collective motion exhibited by solutions of the particle model that result not from changing the control law but from varying key parameters such as the number of neighbors. We call these qualitative changes *bifurcations* and the corresponding parameters *bifurcation parameters*, although rigorous bifurcation analysis is not discussed here.

Bifurcations in models of animal groups is a growing area of research. In [19], bistability of parallel and circular motion is demonstrated in a 3D fish schooling simulation. This bistability generates hysteresis under slow variation of the parameter that determines the outer radius of the orientation zone. Analytical results that provide evidence of bistability of parallel and circular motion in the particle model appear in [30], [31]. If some individuals in a group have differing preferred directions, then the group can bifurcate or split. Simulations suggest that the percentage of informed animals in a group necessary to achieve consensus decreases as the group size increases [32]. Analytical results classifying bifurcations in the phase model when two subgroups of identical individuals have different, preferred directions appears in [33] and, for heterogeneous groups, in [34].

Here we simulate bifurcations that occur in fish schools using biologically realistic parameters in the particle model (1), (2) with the control (22). We assume that the interaction networks generated from perceptual zones may differ for the spacing and orientation controls. In addition, these graphs may be directed and time varying. Analytical results for stabilizing collective motion with directed and time-varying graphs are the subject of [7] using results from [18]. The modified expression of (22) is

$$u_k = \omega_0 + \frac{K_1 - K_0}{N} \langle i e^{i\theta_k}, L_k^{\text{ori}} e^{i\theta} \rangle + \omega_0 \frac{K_0}{N} \langle e^{i\theta_k}, L_k^{\text{att}} \mathbf{r} \rangle. \quad (29)$$

Motivated by [19] and [22], one example of a bifurcation occurs as a result of changing the outer radius of the orientation zone. For simplicity, we assume there is no repulsion zone and that the inner radius of both

the orientation and attraction zones is zero, that is, the orientation and attraction zones overlap. We choose  $\rho_{\text{att}} \gg |\omega_0|^{-1}$ . Let the bifurcation parameter  $\rho = \rho_{\text{ori}} |\omega_0|$  be the ratio of the outer radius of the orientation zone divided by the radius of the circular motion. The angular width of the blind spot is  $\alpha_k = 60^\circ$  for all  $k \in \{1, \dots, N\}$ .

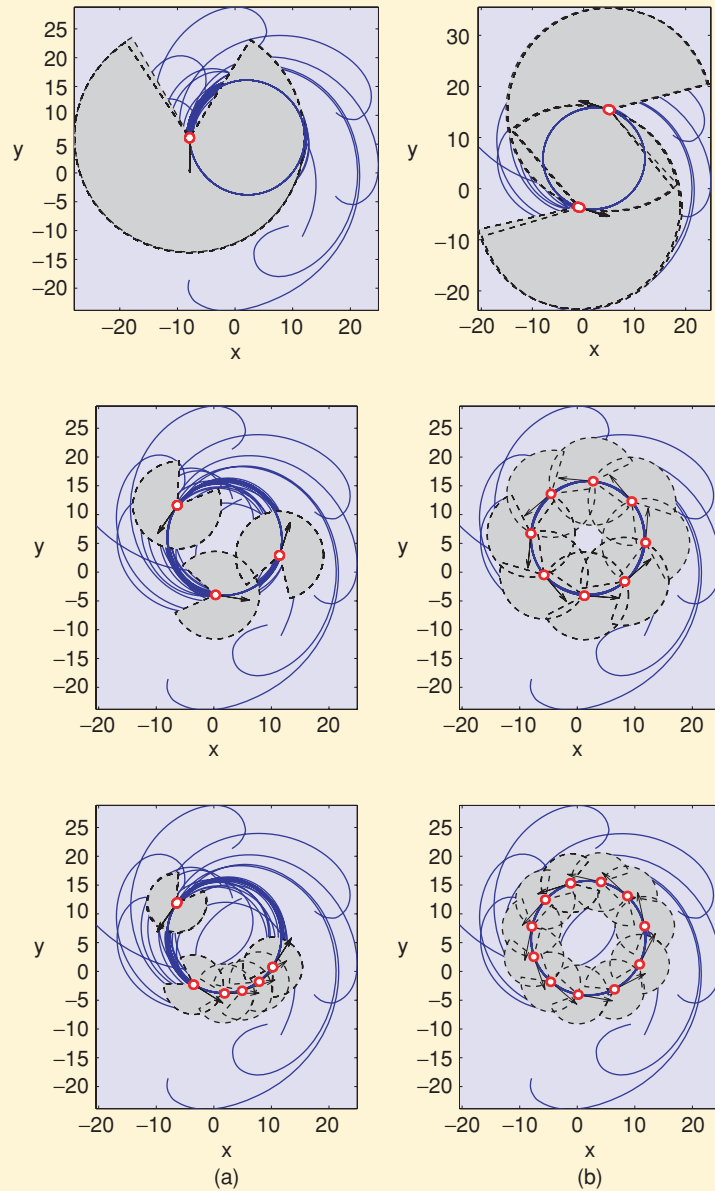


**FIGURE 8** A bifurcation in the circular formation, which occurs as the outer radius of the orientation zone (gray patches) increases. The orientation and spacing interaction networks are generated from the attraction and orientation zones with  $\rho_{\text{att}} \gg |\omega_0|^{-1}$ ,  $\rho_{\text{ori}} = \rho |\omega_0|^{-1}$ , and  $\alpha_k = 60^\circ$ . The control parameters are  $\omega_0 = K_0 = 0.1$ . (a)  $K_1 < 0$  and (b)  $K_1 > 0$ . The rows of the figure from top to bottom correspond to  $\rho = 2 \sin(\pi/M)$ , with  $M = 2$ ,  $M = 8$ , and  $M = 12$ . (a) Increasing the size of the orientation zone stabilizes fewer, larger synchronized clusters of particles; (b) the particles cluster in symmetric patterns.

Under the effect of the spacing control, all of the particles converge to the circular formation shown in Figure 8. For  $K_1 < 0$ , particles in overlapping orientation zones become synchronized. Increasing the size of the orientation zone stabilizes fewer, larger synchronized clusters of particles. This result resembles the bifurcation result of [19] in the following way. Increasing the size of the orientation zone switches the distribution of phases from incoherent or swarm-like to synchronized or parallel. The results differ because, in our simulations, the particles remain in the circular formation, while in [19] the particles switch between swarm-like, circular, and parallel collective motion.

For  $K_1 > 0$ , the particles cluster into the symmetric patterns appropriate for the size of the orientation zone. Because positive gain on the alignment control corresponds to anti-synchronization, clusters form in nonoverlapping orientation zones. We illustrate results for  $\rho_{\text{ori}} = \rho|\omega_0|^{-1}$  and, for  $M = 2, 8,$  and  $12$ ,  $\rho = 2 \sin(\pi/M)$ , which correspond to the chord length that separates  $M$  evenly spaced clusters on a circle of unit radius. Note that, although the clusters are not necessarily equally sized or  $M$  in number, this procedure generates symmetric clusters.

## CONCLUSIONS

This article describes PCOD, a cooperative control framework for stabilizing relative equilibria in a model of self-propelled, steered particles moving in the plane at unit speed. Relative equilibria correspond either to motion of all of the particles in the same direction or to motion of all of the particles around the same circle. Although the framework applies to time-varying and directed interaction between individuals, we focus here on time-invariant and undirected interaction, using the Laplacian matrix of the interaction graph to design a set of decentralized control laws applicable to mobile sensor networks. Since the direction of motion of each particle is represented in the framework by a point on the unit circle, the closed-loop model has coupled-phase oscillator dynamics.

In addition to its application as a design methodology, PCOD can also be used to model and analyze schooling behavior in fish. We illustrate how slow variation of a parameter that determines the radius of interaction between fish generates bifurcations in the collective behavior. The utility of PCOD as a modeling tool is further demonstrated by our analysis of real fish schooling data. Representing the direction of motion of each fish by a point on the unit circle enables us to evaluate the synchronization level of a school and reverse engineer interaction rules that yield the observed schooling pattern. This analysis represents preliminary results from a promising collaboration between biologists and engineers studying collective behavior.

What determines the mechanisms and nature of fish interaction remains an open question. An additional challenge in studying grouping behavior in biological collec-

tives is modeling particles moving in three dimensions at variable speeds. Such models also have potential for improved sensing in air and sea by cooperative control of autonomous vehicles.

## ACKNOWLEDGMENTS

Research was partially supported by a National Science Foundation Graduate Research Fellowship and ONR grants N00014-02-1-0826 and N00014-04-1-0534. This article presents research results of the Belgian Network Dynamical Systems, Control, and Optimization (DYSCO), funded by the Interuniversity Attraction Poles Program, initiated by the Belgian State, Science Policy Office. The scientific responsibility rests with its authors.

## REFERENCES

- [1] C.S. Peskin, *Mathematical Aspects of Heart Physiology* (Courant Institute Lecture Notes). New York: Courant Institute of Mathematical Sciences, 1975.
- [2] N. Kopell and G.B. Ermentrout, "Symmetry and phaselocking in chains of weakly coupled oscillators," *Comm. Pure Appl. Math.*, vol. 39, no. 5, pp. 623–660, 1986.
- [3] S. Watanabe and S. Strogatz, "Constants of motion for superconductor arrays," *Physica D*, vol. 74, no. 3-4, pp. 197–253, 1994.
- [4] A.T. Winfree, "Biological rhythms and the behavior of populations of coupled oscillators," *J. Theor. Biol.*, vol. 16, no. 1, pp. 15–42, 1967.
- [5] Y. Kuramoto, "Self-entrainment of a population of coupled non-linear oscillators," in *Proc. Int. Symp. Mathematical Problems Theoretical Physics*, Jan. 1975, pp. 420–422.
- [6] S.H. Strogatz, "From Kuramoto to Crawford: Exploring the onset of synchronization in populations of coupled oscillators," *Physica D*, vol. 143, no. 1-4, pp. 1–20, 2000.
- [7] R. Sepulchre, D.A. Paley, and N.E. Leonard, "Stabilization of planar collective motion with limited communication," *IEEE Trans. Automat. Contr.*, to be published. [Online]. Available: <http://www.princeton.edu/~naomi>.
- [8] N.E. Leonard, D.A. Paley, F. Lekien, R. Sepulchre, D.M. Fratantoni, and R.E. Davis, "Collective motion, sensor networks and ocean sampling," *Proc. IEEE*, vol. 95, no. 1, pp. 48–74, 2007.
- [9] E. Fiorelli, N.E. Leonard, P. Bhatta, D.A. Paley, R. Bachmayer, and D.M. Fratantoni, "Multi-AUV control and adaptive sampling in Monterey Bay," *IEEE J. Oceanic Eng.*, vol. 31, no. 4, pp. 935–948, Oct. 2006.
- [10] F. Zhang, D.M. Fratantoni, D.A. Paley, J.M. Lund, and N.E. Leonard, "Control of coordinated patterns for ocean sampling," *Int. J. Contr.* [Online]. Available: <http://www.princeton.edu/~naomi>.
- [11] A. Okubo, "Dynamical aspects of animal grouping: Swarms, schools, flocks, and herds," *Adv. Biophys.*, vol. 22, pp. 1–94, 1986.
- [12] D. Grünbaum and A. Okubo, "Modelling social animal aggregations," in *Lecture Notes in Biomathematics 100*, S.A. Levin, Ed. Berlin: Springer-Verlag, 1994, pp. 296–325.
- [13] D. Grünbaum, "Schooling as a strategy for taxis in a noisy environment," *Evolutionary Ecology*, vol. 12, no. 5, pp. 503–522, 1998.
- [14] G. Flierl, D. Grünbaum, S. Levin, and D. Olson, "From individuals to aggregations: The interplay between behavior and physics," *J. Theor. Biol.*, vol. 196, no. 4, pp. 397–454, 1999.
- [15] E.W. Justh and P.S. Krishnaprasad, "Equilibria and steering laws for planar formations," *Syst. Control Lett.*, vol. 52, no. 1, pp. 25–38, 2004.
- [16] A. Jadbabaie, J. Lin, and A.S. Morse, "Coordination of groups of mobile autonomous agents using nearest neighbor rules," *IEEE Trans. Automat. Contr.*, vol. 48, no. 6, pp. 988–1001, 2003.
- [17] R. Olfati-Saber and R.M. Murray, "Consensus problems in networks of agents with switching topology and time-delays," *IEEE Trans. Automat. Contr.*, vol. 49, no. 9, pp. 1520–1533, 2004.
- [18] L. Moreau, "Stability of multiagent systems with time-dependent communication links," *IEEE Trans. Automat. Contr.*, vol. 50, no. 2, pp. 169–182, 2005.
- [19] I.D. Couzin, J. Krause, R. James, G.D. Ruxton, and N.R. Franks, "Collective memory and spatial sorting in animal groups," *J. Theor. Biol.*, vol. 218, no. 1, pp. 1–11, 2002.

- [20] S.V. Viscido, J.K. Parrish, and D. Grünbaum, "Individual behavior and emergent properties of fish schools: A comparison of observation and theory," *Marine Ecology Progress Series*, vol. 273, pp. 239–249, June 8, 2004.
- [21] D. Grünbaum, S. Viscido, and J.K. Parrish, "Extracting interactive control algorithms from group dynamics of schooling fish, in *Cooperative Control: A Post-Workshop Volume 2003 Block Island Workshop on Cooperative Control*, V. Kumar, N. Leonard, and A.S. Morse, Eds. Springer-Verlag, 2005, pp. 104–117.
- [22] S.V. Viscido, J.K. Parrish, and D. Grünbaum, "The effect of population size and number of influential neighbors on the emergent properties of fish schools," *Ecological Modelling*, vol. 183, no. 2-3, pp. 347–363, 2005.
- [23] Y. Kuramoto, *Chemical Oscillations, Waves, and Turbulence*. New York: Springer-Verlag, 1984.
- [24] N. Moshtagh and A. Jadbabaie, "Distributed geodesic control laws for flocking of nonholonomic agents," *IEEE Trans. Automat. Contr.*, vol. 52, no. 4, pp. 681–686, 2007.
- [25] R. Sepulchre, D. Paley, and N.E. Leonard, "Stabilization of planar collective motion: All-to-all communication," *IEEE Trans. Automat. Contr.*, vol. 52, no. 5, pp. 104–117, 2007.
- [26] R. Sepulchre, D. Paley, and N.E. Leonard, "Graph Laplacian and Lyapunov design of collective planar motions," in *Proc. Int. Symp. Nonlinear Theory Applications*, Bruges, Belgium, Oct. 2005, pp. 217–232.
- [27] R. Sepulchre, D.A. Paley, and N.E. Leonard, "Group coordination and cooperative control of steered particles in the plane, in *Group Coordination and Cooperative Control*," (Lecture Notes in Control and Information Sciences no. 336), K.Y. Pettersen, J.T. Gravdahl, and H. Nijmeijer, Eds. New York: Springer-Verlag, 2006, pp. 217–232.
- [28] J. Jeanne, N.E. Leonard, and D. Paley, "Collective motion of ring-coupled planar particles," in *Proc. 44th IEEE Conf. Decision Control*, Seville, Spain, Dec. 2005, pp. 3929–3934.
- [29] D.A. Paley, N.E. Leonard, and R. Sepulchre, "Collective motion of self-propelled particles: Stabilizing symmetric formations on closed curves," in *Proc. 45th IEEE Conf. Decision Control*, San Diego, CA, Dec. 2006, pp. 5067–5072.
- [30] D. Paley, N.E. Leonard, and R. Sepulchre, "Collective motion: Bistability and trajectory tracking," in *Proc. 43rd IEEE Conf. Decision Control*, Nassau, Bahamas, Dec. 2004, pp. 1932–1937.
- [31] D.A. Paley, N.E. Leonard, R. Sepulchre, and I.D. Couzin, "Spatial models of bistability in biological collectives," preprint [Online]. Available: <http://www.princeton.edu/~dpaley>
- [32] I.D. Couzin, J. Krause, N.R. Franks, and S.A. Levin, "Information transfer, decision-making, and leadership in animal groups," *Nature*, vol. 433, no. 7025, pp. 513–516, 2004.
- [33] B. Nabet, N.E. Leonard, I. Couzin, and S. Levin, "Leadership in animal group motion: A bifurcation analysis," in *Proc. 17th Int. Symp. Mathematical Theory Networks Systems*, Kyoto, Japan, July 2006, pp. 1–14.
- [34] S.J. Moon, B. Nabet, N.E. Leonard, S.A. Levin, and I.G. Kevrekidis, "Heterogeneous animal group models and their group-level alignment dynamics: An equation-free approach," *J. Theoretical Biol.*, vol. 246, no. 1, pp. 100–112, 2007.
- [35] R.A. Horn and C.R. Johnson, *Matrix Analysis*. Cambridge, U.K.: Cambridge Univ. Press, 1985.
- [36] E.W. Weisstein, Circulant graph. MathWorld—A Wolfram Web [Online]. Available: <http://mathworld.wolfram.com/CirculantGraph.html>
- [37] J.A. Fax and R.M. Murray, "Information flow and cooperative control of vehicle formations," *IEEE Trans. Automat. Contr.*, vol. 49, no. 9, pp. 1465–1476, 2004.
- [38] R.M. Gray, "Toeplitz and circulant matrices: A review," *Found. Trends Commun. Inform. Theory*, vol. 2, no. 3, pp. 155–239, 2006.

## AUTHOR INFORMATION

**Derek A. Paley** (dpaley@princeton.edu) is a Ph.D. candidate in the Department of Mechanical and Aerospace Engineering of Princeton University. He received the B.S. degree in applied physics from Yale University in 1997. From 1997 to 2000, he worked as an analyst for Metron, Inc. From 2000 to 2002, he worked as a software engineer in the underwater vehicle industry for Bluefin Robotics Corp. He received the M.A. degree in mechanical and aerospace engineering from Princeton University in 2004.

His research interests include collective motion in natural and engineered systems, cooperative control, and marine robotics. He can be contacted at Princeton University, Department of Mechanical and Aerospace Engineering, Princeton, NJ 08544 USA.

**Naomi Ehrich Leonard** is a professor in the Mechanical and Aerospace Engineering Department and an associated faculty member of the Program in Applied and Computational Mathematics at Princeton University. She received the B.S.E. degree in mechanical engineering from Princeton University in 1985. From 1985 to 1989, she worked as an engineer in the electric power industry for MPR Associates, Inc. She received the M.S. and Ph.D. degrees in electrical engineering from the University of Maryland, College Park, in 1991 and 1994. Her research interests include nonlinear control and dynamics, cooperative control, mobile sensor networks, autonomous underwater vehicles, adaptive ocean sampling, and collective motion in animal aggregations.

**Rodolphe Sepulchre** is a professor in the Department Electrical Engineering and Computer Science at the University of Liège, Belgium. He received his engineering degree and Ph.D. degree in applied mathematics from the University of Louvain, Belgium, in 1990 and 1994, respectively. He held a postdoctoral position at the University of California, Santa Barbara, and a visiting position at Princeton University. His research focuses on theory and applications of nonlinear dynamical systems. He is a coauthor of *Constructive Nonlinear Control* (Springer-Verlag, 1997). He serves as an associate editor for the journal *Mathematics of Control, Signals, and Systems*.

**Daniel Grünbaum** is an associate professor in the School of Oceanography and an adjunct associate professor in the Department of Biology at the University of Washington. He received a B.S. in mechanical engineering from the University of Washington in 1983. He received a Ph.D. from Cornell University in ecology and evolutionary biology in 1992. He was a research associate in the Department of Zoology, a Killam Postdoctoral Fellow at the University of British Columbia, and a visiting assistant professor at the University of Utah. His interests include the biomechanics and behavior of organisms as well as their linkages to the dynamics and evolution of ecological systems.

**Julia K. Parrish** is an associate professor in the Biology Department as well as associate director of the School of Aquatic and Fishery Sciences, at the University of Washington. She received her Ph.D. in zoology from Duke University in 1988, and studied schooling in fish and other open ocean organisms at the University of California, Los Angeles. She is a coeditor of *Animal Groups in Three Dimensions* (Cambridge University Press, 1997). Her research focuses on the interplay between individual animal behavior and movement, and resultant pattern at the group level. She is a fellow of the American Ornithological Union. 